

UC Irvine

UC Irvine Previously Published Works

Title

Study of noncollinear two-charged-particle events produced in 29-GeV electron-positron annihilation.

Permalink

<https://escholarship.org/uc/item/32q840jk>

Journal

Physical review. D, Particles and fields, 34(11)

ISSN

0556-2821

Authors

Perl, ML
Müller, L
Barklow, T
[et al.](#)

Publication Date

1986-12-01

DOI

10.1103/physrevd.34.3321

Copyright Information

This work is made available under the terms of a Creative Commons Attribution License, available at <https://creativecommons.org/licenses/by/4.0/>

Peer reviewed

Study of noncollinear two-charged-particle events produced in 29-GeV electron-positron annihilation

M. L. Perl, L. Müller, T. Barklow, A. M. Boyarski, M. Breidenbach, P. R. Burchat, D. L. Burke, J. M. Dorfan, G. J. Feldman, L. Gladney,^(a) G. Hanson, K. Hayes, R. J. Hollebeek, W. R. Innes, J. A. Jaros, D. Karlen, A. J. Lankford, R. R. Larsen, B. W. LeClaire, N. S. Lockyer,^(a) V. Lüth, C. Matteuzzi,^(b) R. A. Ong, B. Richter, K. Riles, M. C. Ross, D. Schlatter,^(b) J. M. Yelton,^(c) and C. Zaiser
Stanford Linear Accelerator Center, Stanford University, Stanford, California 94305

G. S. Abrams, D. Amidei,^(d) A. R. Baden, J. Boyer, F. Butler, G. Gidal, M. K. Gold, G. Goldhaber, L. Golding,^(e) J. Haggerty, D. Herrup, I. Juricic, J. A. Kadyk, M. E. Nelson,^(f) P. C. Rowson, H. Schellman,^(g) W. B. Schmidke, P. D. Sheldon, C. de la Vaissiere,^(h) and D. R. Wood

Lawrence Berkeley Laboratory and Department of Physics, University of California, Berkeley, California 94720

M. E. Levi⁽ⁱ⁾ and T. Schaad

Department of Physics, Harvard University, Cambridge, Massachusetts 02138

(Received 2 June 1986)

This paper presents a study of events produced in 29-GeV electron-positron annihilation in which there are just two noncollinear charged particles, no detected photons, and two or more undetected particles. These events can be explained by attributing them primarily to the reactions $e^+e^- \rightarrow e^+e^-e^+e^-$ and $e^+e^- \rightarrow e^+e^-\mu^+\mu^-$ where just two particles appear in the Mark II detector. There is no evidence for unconventional sources for such events.

I. INTRODUCTION

We have used the Mark II detector to study a class of noncollinear, two-charged-particle events without detected photons produced in 29-GeV electron-positron annihilation. This class consists of events with two or more undetected particles. We find that the bulk of these events can be explained by attributing them to the reactions $e^+e^- \rightarrow e^+e^-e^+e^-$, $e^+e^- \rightarrow e^+e^-\mu^+\mu^-$, and $e^+e^- \rightarrow \gamma\gamma e^+e^-$ where just two charged particles are detected in the Mark II detector. The reaction $e^+e^- \rightarrow \tau^+\tau^-$ where only two charged particles and neutrinos are produced in the τ decays also contributes. We present quantitative comparisons of the cross sections for these reactions with the measured cross sections. There is no evidence for an unconventional source for any of the events. However the relatively large cross sections of the known reactions and the solid-angle limitations of the Mark II detector make it difficult to set significant limits on unconventional reactions that could produce such events. The data were obtained at the PEP electron-positron collider at the Stanford Linear Accelerator Center.

There are three reasons for this study. First, recent work of Berends, Daverveldt, and Kleiss^{1,2} has provided exact matrix elements and convenient computer programs for calculating the cross sections and properties of the reactions $e^+e^- \rightarrow e^+e^-e^+e^-$, $e^+e^-\mu^+\mu^-$. We were interested in comparing their work with our measurements in the special kinematic region occupied by the noncol-

linear events. Second, in a previous study³ we used these events to set upper limits on heavy-neutral-lepton production in e^+e^- annihilation. These events limited the sensitivity of that search, and it is important to understand their origin. Third, there will be searches for heavy neutral leptons or other unexpected particles in noncollinear events at higher-energy e^+e^- colliders: KEK's TRISTAN, CERN's LEP, and the SLAC Linear Collider. We wanted to establish experimental methods for studying the contributions of conventional processes to such events.

The studied events have a collinearity angle (θ_{coll} defined in Fig. 1) greater than 20° , each charged track has a momentum greater than 1.0 GeV/c, and the total charge is zero. There are no detected, isolated photons in the event with energies above 0.3 GeV. However, the Mark II apparatus did not detect photons in certain angular regions, such as close to the beamline. The reasons for the θ_{coll} and momentum criteria are given in Sec. III. Those criteria lead to almost all events having an invariant pair mass larger than 1.0 GeV/c². Therefore in the comparison of the data with theory it is convenient to impose the criterion that the invariant mass be larger than 1.0 GeV/c².

The plan of this paper is as follows. The apparatus and the initial event-selection criteria are described in Sec. II. Some kinematic properties of the data and the final event-selection criteria are presented in Sec. III. The data are compared to the reactions $e^+e^- \rightarrow e^+e^-e^+e^-$, $e^+e^-\mu^+\mu^-$, $e^+e^- \rightarrow \gamma\gamma e^+e^-$, and $e^+e^- \rightarrow \tau^+\tau^-$ in Sec. IV, and the paper is summarized in Sec. V.

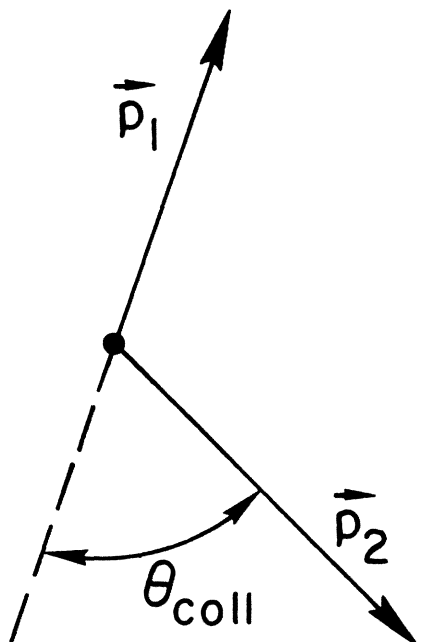


FIG. 1. Definition of θ_{coll} . The p_i 's are the charged-particle momentum vectors.

II. APPARATUS AND INITIAL EVENT SELECTION

A. Apparatus

The Mark II detector, Fig. 2, was used at the PEP electron-positron collider at the Stanford Linear Accelerator Center. Here we emphasize a few properties of the detector pertinent to the search described in this paper.

(1) The main drift-chamber tracks particles reliably over about 80% of the 4π solid angle. The charged particles of the events used were required to be within a slight-

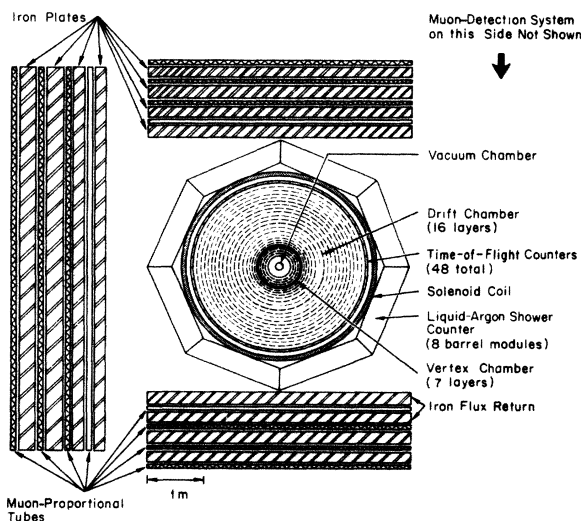


FIG. 2. Cross-section view of Mark II detector.

ly smaller solid angle: namely, 68% of 4π .

(2) The liquid-argon electromagnetic calorimeter, used to detect electrons and photons, covers about 70% of the 4π solid angle.

(3) The lead sheet and proportional chamber detectors (two layers each) at each end of the detector, called end cap chambers, cover the polar angular region from about 15° to 40° . These end-cap chambers detect both photons and charged particles.

(4) The photon detection system is incomplete since (i) there is a gap about 5° in polar angle between the liquid-argon calorimeter and the end-cap calorimeter, (ii) the liquid-argon calorimeter has eight separate modules with longitudinal walls separating the modules, and (iii) the end-cap chambers themselves have gaps in their angular coverage.

(5) The muon-detection system covers about 45% of the 4π solid angle.

B. Data acquisition

The 29-GeV data set used in this study comes from an integrated luminosity of 29.3 pb^{-1} . We use this data set, rather than our total data corresponding to a luminosity of 220 pb^{-1} , because the raw data tapes in this set were processed for all two-charged-particle events which triggered the detector.

The trigger requirements relevant to two-charged-particle events without isolated photons are listed next. At least one of the following trigger conditions had to occur.

(1) Two particle tracks in the main drift chamber had to be found by a hardware track processor within the center 75% of the 4π solid angle. The momentum of each track had to be larger than $50 \text{ MeV}/c$ and the θ_{coll} less than roughly 175° (see Fig. 1).

(2) At least two liquid-argon or end-cap modules had to have a deposition of electromagnetic shower energy over threshold; the threshold was about 1 GeV for liquid-argon modules and about 3 GeV for end-cap modules.

(3) One track as described in (1) had to be found and one calorimeter module had to be over the threshold described in (2).

Trigger conditions (2) and (3), are relevant when one or both particles are electrons.

C. Event selection

Events were selected by the following criteria

(1) The event's vertex is inside a cylinder of 4-cm radius centered on the interaction point.

(2) There are exactly two charge particles with total charge zero in the main drift chamber.

(3) Each particle has $|\cos\theta| < 0.68$ where θ is the angle between the particle's initial vector momentum \mathbf{p} and the beam axis. This criterion means that particles are reliably tracked in the drift chamber, and enter the fiducial volume of the liquid-argon calorimeter.

(4) Each particle has $1.0 \leq p \leq 20.0 \text{ GeV}/c$ where p is the magnitude of \mathbf{p} . The upper limit of $20.0 \text{ GeV}/c$ allows for a measurement error of about two standard deviations for the most energetic particles.

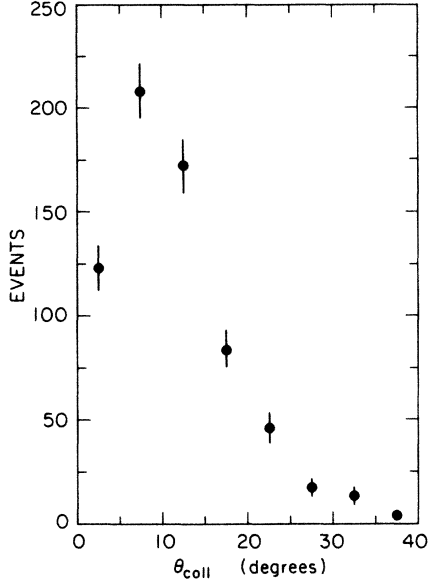


FIG. 3. The calculated θ_{coll} distribution for the zero-photon $e^+e^- \rightarrow \tau^+\tau^-$ reaction using a Monte Carlo method. Of the 680 produced events, 13 have $\theta_{\text{coll}} > 40^\circ$ and are not shown.

(5) $\theta_{\text{coll}} > 20^\circ$.

(6) There are no isolated photons in the liquid-argon calorimeter. An isolated photon lies sufficiently far from all charged tracks so that $\cos\theta_{\gamma j} < 0.99$, $\theta_{\gamma j}$ being the angle between the momentum vector of the photon \mathbf{p}_γ and that of the charged particle j , \mathbf{p}_j . In addition an isolated photon is required to have an energy $E_\gamma > 0.3$ GeV.

(7) There are no photons with $E_\gamma > 0.3$ GeV detected in the end-cap chambers.

(8) For convenience we list here one additional criterion which is explained in Sec. III B. The invariant mass of the pair of charged particles is larger than 1.0 GeV/ c^2 . (This assumes the particles are e , μ , or π so that their rest mass can be ignored.)

The criteria $\theta_{\text{coll}} > 20^\circ$ and $p > 1.0$ GeV/ c exclude most of the zero-photon, two-charged-particle events produced in 29 GeV e^+e^- annihilation. Hence we must explain their use. The θ_{coll} criterion is used to remove the bulk of the $e^+e^- \rightarrow e^+e^-$, $e^+e^- \rightarrow \mu^+\mu^-$, and zero-photon $e^+e^- \rightarrow \tau^+\tau^-$ events. In the zero-photon $e^+e^- \rightarrow \tau^+\tau^-$ case (Fig. 3) about 14% of the events survive this criterion. The $p > 1.0$ GeV/ c criterion is imposed to allow electrons to be identified with reasonable efficiency. Muon identification requires higher p and occurs in a more restricted solid angle.

III. KINEMATIC PROPERTIES AND FINAL EVENT SELECTION

A. Kinematic variables

Denoting the two charged particles by 1 and 2, the event can be described by the six momentum components of \mathbf{p}_1 and \mathbf{p}_2 . But the physics of the reactions to be studied suggests that other kinematic variables are of more

direct interest. These variables are as follows.

(1) The collinearity angle θ_{coll} that has been defined.

(2) The invariant mass m of the pair which is given by

$$\begin{aligned} m^2 &= (p_1 + p_2)^2 - (\mathbf{p}_1 + \mathbf{p}_2)^2 \\ &= 2p_1 p_2 (1 + \cos\theta_{\text{coll}}) \end{aligned} \quad (1)$$

when we set the masses of the particles to zero. We do so here because almost all the particles are expected to be e 's, μ 's, or π 's, because we will eventually set $m \geq 1.0$ GeV/ c^2 , and because often we cannot identify a particle.

(3) The transverse momentum p_T , which is given by

$$p_T^2 = (p_{1x} + p_{2x})^2 + (p_{1y} + p_{2y})^2 \quad (2)$$

where the z axis lies along the beam direction.

(4) The invariant mass of the undetected particles, m_{miss} , which is given by

$$(m_{\text{miss}})^2 = (E_{\text{c.m.}} - p_1 - p_2)^2 - (\mathbf{p}_1 + \mathbf{p}_2)^2, \quad (3)$$

where $E_{\text{c.m.}}$ is the total energy, 29 GeV. The variable $(m_{\text{miss}})^2$ is difficult to use since its distribution due to measurement errors or initial-state radiation is asymmetric. Therefore we use the related quantity Δ which has a more symmetric error distribution (see, for example, Fig. 9).

(5) We define

$$\Delta = E_{\text{miss}} - p_{\text{miss}}, \quad (4a)$$

where

$$E_{\text{miss}} = E_{\text{c.m.}} - p_1 - p_2,$$

$$p_{\text{miss}} = |\mathbf{p}_1 + \mathbf{p}_2|.$$

Thus

$$\Delta = (m_{\text{miss}})^2 / (E_{\text{miss}} + p_{\text{miss}}) \quad (4b)$$

and

$$\Delta = 0 \quad \text{when } m_{\text{miss}} = 0.$$

B. Distribution of kinematic variables and final event selection

Figures 4 and 5 give the m and θ_{coll} distributions excluding event criterion 8. The existence of very few

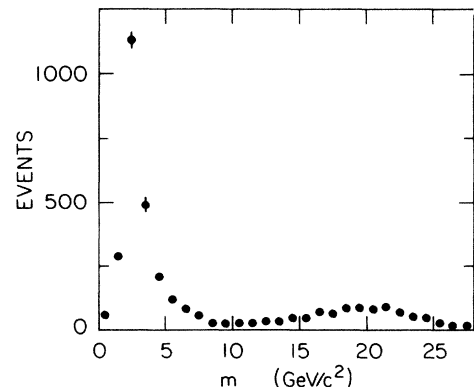


FIG. 4. The measured pair-mass m distribution before the criterion $m > 1.0$ GeV/ c^2 is imposed.

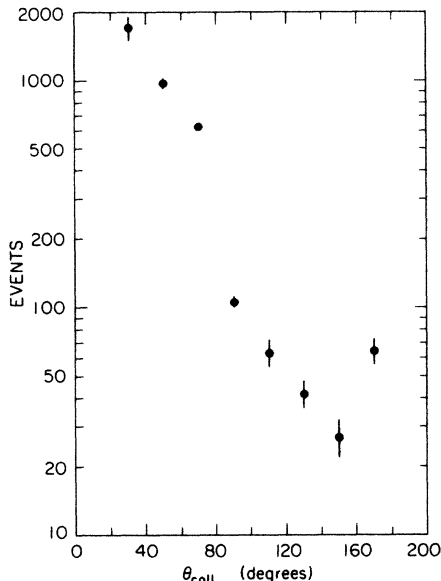


FIG. 5. The measured θ_{coll} distribution before the criterion $m > 1.0 \text{ GeV}/c^2$ is imposed. The criterion $\theta_{\text{coll}} > 20^\circ$ has already been imposed.

events with $m < 1.0 \text{ GeV}/c^2$ is a result of the $p > 1.0 \text{ GeV}/c$ criterion and the small number of events with $\theta_{\text{coll}} > 120^\circ$. As discussed in Sec. IV, our use of the Monte Carlo computer programs for $e^+e^- \rightarrow e^+e^-e^+e^-$, $e^+e^- \mu^+\mu^-$ requires setting a lower limit for m . It is therefore convenient to set a final event-selection criterion:

$$m > 1.0 \text{ GeV}/c^2. \quad (5)$$

Imposing this criterion leaves 3393 events.

C. Separation of events

There are two known classes of reactions that can yield the type of events under study. Class 1 consists of $e^+e^- \rightarrow e^+e^- \gamma, \mu^+\mu^- \gamma$ with the γ undetected; hence the missing invariant mass is zero. Class 2 consists

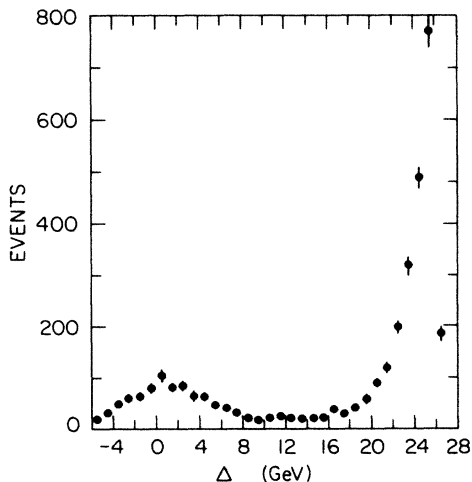


FIG. 6. The measured Δ distribution.

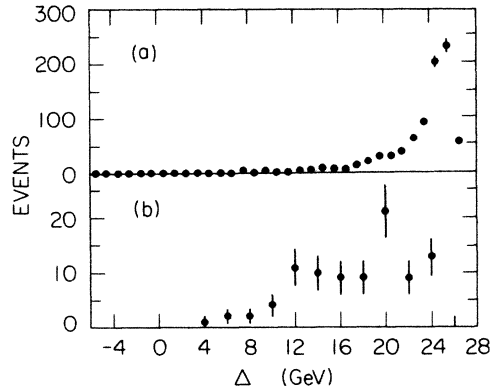


FIG. 7. The calculated Δ distribution for (a) $e^+e^- \rightarrow e^+e^-e^+e^-$, and (b) zero-photon $e^+e^- \rightarrow \tau^+\tau^-$.

of $e^+e^- \rightarrow e^+e^-e^+e^-$, $e^+e^- \mu^+\mu^-$, $\gamma\gamma e^+e^-$, $e^+e^- \pi^+\pi^-$, and zero-photon $e^+e^- \rightarrow \tau^+\tau^-$, where at least two particles are undetected and the missing invariant mass is larger than zero. Using the parameter Δ , Eq. (4), we find that the Δ distribution of the data, Fig. 6, separates into two well-defined peaks.

Figure 7 shows the calculated Δ distribution for $e^+e^- \rightarrow e^+e^-e^+e^-$ and zero-photon $e^+e^- \rightarrow \tau^+\tau^-$ events that meet all of the event-selection criteria. The $e^+e^- \rightarrow e^+e^-e^+e^-$ was obtained from the Monte Carlo computer programs described in Sec. IV A; the $e^+e^- \rightarrow \tau^+\tau^-$ prediction was obtained from a Monte Carlo program called HOWLTAU used by our collaboration. We observe that in these class-2 reactions, almost all events have Δ larger than 10. The peaking at near maximum Δ in $e^+e^- \rightarrow e^+e^-e^+e^-$ is caused by the small values of p_1 and p_2 , Fig. 8. On the other hand, we can

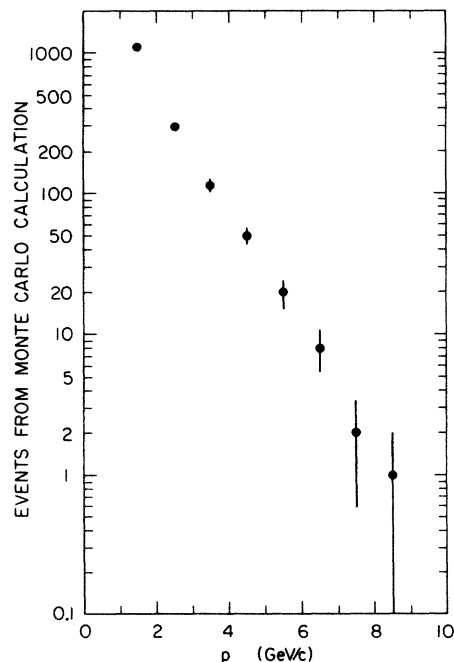


FIG. 8. The calculated momentum distribution for $e^+e^- \rightarrow e^+e^-e^+e^-$. Here $p = p_1$ or p_2 .

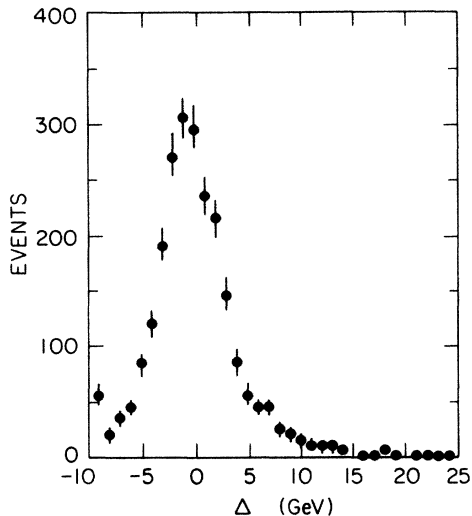


FIG. 9. The measured Δ distribution for $e^+e^- \rightarrow e^+e^-\gamma$ events where all three final-state particles are detected and the total detected energy is greater than 20 GeV. This distribution is taken from a much larger data sample.

obtain an experimental Δ distribution for class-1 reactions by using events which meet all criteria except the no-photon criterion 6 in Sec. II C. That criterion is replaced by the requirement that there be one and only one isolated photon detected in the liquid-argon calorimeter. The Δ distribution of these events (Fig. 9) shows that most class-1 events will have Δ less than about 10 GeV. It is important to use a measured distribution here in order to fully take account of the effect of the detector resolution when the missing mass is zero. The width and shape of this distribution is discussed in Appendix A.

The goal is to choose a value of Δ , called Δ_{sep} , that best separates the two classes of events. Unfortunately there is a correlation between Δ and m which depends upon $p_{\text{tot}} = |\mathbf{p}_1 + \mathbf{p}_2|$. This is shown in the measured Δ - m distribution in Table I and is illustrated in Fig. 10. The correlation can be understood by considering the case of p_{tot} being much smaller than $E = |\mathbf{p}_1| + |\mathbf{p}_2|$. Then

$$m \approx E - p_{\text{tot}}^2/2E.$$

Since

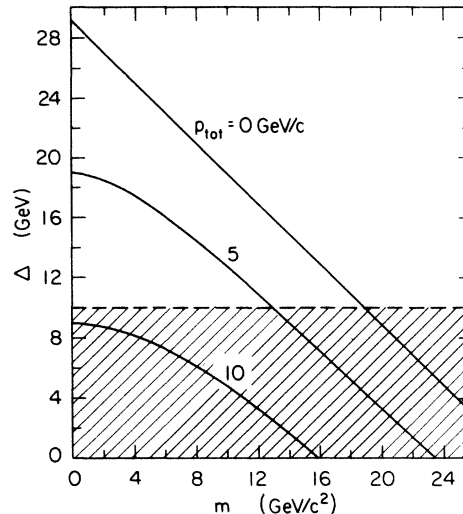


FIG. 10. The relation between Δ , m , and p_{tot} . The unshaded area shows the acceptance region for these variables when $\Delta_{\text{sep}} = 10$ GeV. If there were no measurement errors, class-1 events have $\Delta = 0$.

$$\Delta = E_{\text{c.m.}} - E - p_{\text{tot}}$$

then

$$m \approx E_{\text{c.m.}} - p_{\text{tot}}^2/2E - p_{\text{tot}} - \Delta, \quad (6)$$

and when $p_{\text{tot}} = 0$,

$$m_{\text{max}} = E_{\text{c.m.}} - \Delta.$$

Thus large values of m , say about 10 or 15 GeV require small values of Δ . But Fig. 9 indicates that Δ_{sep} must be at least as large as, say, 10 GeV to exclude most class-1 events from the class-2 region. Indeed we choose $\Delta_{\text{sep}} = 10$ GeV. This means there can be some contamination of class-2 events by class-1 events. Figure 10 shows that $\Delta_{\text{sep}} = 10$ GeV yields good acceptance when m and p_{tot} are in their lower range of values. Most of the events considered in this paper have such m and p_{tot} values. However $\Delta_{\text{sep}} = 10$ GeV severely limits the acceptance for large values of m or p_{tot} . There is nothing we can do about this limitation in the analysis technique used in this

TABLE I. Numbers of events in the measured joint m - Δ distribution. About $\frac{1}{4}$ of the data is shown here. Blank spaces indicate zero events.

Δ (GeV) \ m (GeV/c ²)	0-4	4-8	8-12	12-16	16-20	20-24	24-28
(-10)-(-5)			2	1	1	2	8
(-5)-0					14	36	22
0-5			3	18	54	27	
5-10	1	3	7	16	14		
10-15	2	7	6	5			
15-20	7	17	4				
20-25	229	69					
25-30	149						

work. The incomplete photon detection of our detector forces us to use the Δ separation method, or an equivalent method. And then the measurement errors discussed in Appendix A require a large value of Δ_{sep} .

A detailed analysis of $e^+e^- \rightarrow e^+e^-\gamma, \mu^+\mu^-\gamma$ with an undetected γ is related to a study of those events with the γ detected which is being carried out by one of us (M.K.G.). The incompleteness of the Mark II photon detection system makes the study of the former type of events dependent on a study of the latter type. Therefore at this point we remove events with $\Delta < 10.0$ GeV from the sample. Preliminary analysis indicates that many of these $\Delta < 10.0$ GeV events are from $e^+e^- \rightarrow e^+e^-\gamma$ or $e^+e^- \rightarrow \mu^+\mu^-\gamma$ but we must wait for a detailed analysis to make this indication quantitative.

IV. EVENTS WITH TWO OR MORE UNDETECTED PARTICLES

In this section we compare events that might have two or more undetected particles, specifically events with $\Delta > 10$ GeV, with possible sources for such events. There are about 2400 such events.

A. Calculations for e^+e^- and $\mu^+\mu^-$ pairs from $e^+e^- \rightarrow e^+e^-e^+e^-$, $e^+e^-\mu^+\mu^-$

We calculated the cross section and kinematic variable distributions for e^+e^- and $\mu^+\mu^-$ pairs from the reactions

$$e^+ + e^- \rightarrow e^+ + e^- + e^+ + e^- \quad (7a)$$

and

$$e^+ + e^- \rightarrow e^+ + e^- + \mu^+ + \mu^- \quad (7b)$$

that meet the event criteria of Sec. IIC. We used the Berends, Daverveldt, and Kleiss^{1,2} Monte Carlo computer program entitled "No Tagging." In this computation method the matrix elements are first replaced by approximate analytic expressions. These analytic expressions are then used to produce events through the Monte Carlo importance sampling method. Next, each event is weighted by the ratio of the exact matrix element cross section to the approximate matrix element cross section for that event. Finally, a Monte Carlo rejection method is used on those weights to produce a set of unweighted events.

In general, detector acceptance factors and event-selection criteria cannot be applied inside the computation process, but must be applied to the final set of unweighted events. There is one exception which is easier to explain in the $e^+e^- \rightarrow e^+e^-\mu^+\mu^-$ case. One can set the minimum and maximum values of the invariant mass of the $\mu^+\mu^-$ pair, $m_{\mu^+\mu^-}$. The importance sampling produces events with $m_{\mu^+\mu^-}$ between the selected maximum and minimum values. In our computations for the reaction $e^+e^- \rightarrow e^+e^-\mu^+\mu^-$ we set minimum values for $m_{\mu^+\mu^-}$ in order to obtain a sufficient number of events which met the event-selection criteria $m > 1.0$ GeV/ c^2 .

In the calculation of events for the reaction $e^+e^- \rightarrow e^+e^-e^+e^-$, minimum and maximum values of $m_{e^+e^-}$ can also be set. However in this case these limits apply to all four e^+e^- pairs. Since our $m > 1.0$ GeV/ c event-selection criteria applies only to the observed e^+e^- , setting a minimum value of $m_{e^+e^-}$ at 1.0 GeV/ c will lead to a calculated cross section smaller than that set by the event criteria. However, in a similar situation the error was estimated² to be less than 1%.

Using these methods we produced sets of unweighted events for $e^+e^- \rightarrow e^+e^-e^+e^-$ and $e^+e^- \rightarrow e^+e^-\mu^+\mu^-$; about 1500 events in each set met the event criteria in Sec. IIC. The event criteria restrict the reactions in Eq. (7) to a very small part of the kinematic region available to these reactions, as is illustrated in Table II. Most of the total cross section is occupied by final states in which an e^+ and an e^- are emitted very close to the respective directions of the initial state e^+ and e^- , respectively, the momenta of the other two final-state particles being very small. The $e^+e^-e^+e^-$ total cross section is much larger than the $e^+e^-\mu^+\mu^-$ total cross section, but once the criterion that $m \geq 1$ GeV/ c^2 is applied, the cross sections are the same magnitude. The imposition of the other criteria leads to approximately equal cross sections for the $e^+e^-e^+e^-$ and $e^+e^-\mu^+\mu^-$ final states throughout the kinematic region allowed by the event criteria, Tables II and III. We note that the criteria listed in Sec. IIC severely reduce the cross sections.

Almost all the Monte Carlo events which meet the event criteria are produced by the multiperipheral diagrams, Fig. 11(a), in the terminology of Berends, Daverveldt, and Kleiss. The remainder of the events, of the order of a percent, are produced by the bremsstrahlung diagrams, Fig. 11(b).

TABLE II. Calculated cross sections for $e^+e^- \rightarrow e^+e^-e^+e^-$ and $e^+e^- \rightarrow e^+e^-\mu^+\mu^-$.

Restrictions on cross section	Cross section (pb)	
	$e^+e^- \rightarrow e^+e^-e^+e^-$	$e^+e^- \rightarrow e^+e^-\mu^+\mu^-$
none	1.1×10^{10}	1.2×10^5
$m \geq 1$ GeV/ c	16700 ± 160	9570 ± 110
$m \geq 2$ GeV/ c	2940 ± 10	2110 ± 10
$m \geq 1$ GeV/ c^2 and criteria of Sec. IIC	53.7 ± 2.4	53.8 ± 2.1
$m \geq 2$ GeV/ c^2 and criteria of Sec. IIC	47.9 ± 1.7	47.2 ± 1.6
$m \geq 5$ GeV/ c^2 and criteria of Sec. IIC	5.4 ± 0.5	5.2 ± 0.5

TABLE III. Calculated cross sections in pb for the indicated process and kinematic regions. The event criteria of Sec. II C and the criterion $\Delta > 10$ GeV are imposed. A blank space indicates no Monte Carlo events.

m range (GeV/ c^2)	p_T range (GeV/ c)	$e^+e^- \rightarrow \tau^+\tau^-$		
		$e^+e^- \rightarrow e^+e^-e^+e^-$	$e^+e^- \rightarrow e^+e^-\mu^+\mu^-$	2 prong, 0 photon
1-2	0-1	5.3±1.7	4.8±1.1	
	1-3		1.3±0.6	
	3-9	0.44±0.44	0.51±0.36	
2-3	0-1	24.1±1.2	23.2±1.1	0.02±0.02
	1-3	1.9±0.3	2.2±0.4	
	3-9	0.25±0.18	0.25±0.14	
3-5	0-1	13.2±0.7	11.8±0.7	0.06±0.04
	1-3	2.9±0.3	3.0±0.4	0.43±0.09
	3-9	0.65±0.16	0.53±0.15	0.06±0.04
5-10	0-1	3.6±0.4	2.8±0.4	0.14±0.05
	1-3	1.1±0.2	1.3±0.2	0.43±0.09
	3-9	0.45±0.13	0.66±0.17	0.48±0.10
10-15	0-1	0.12±0.07	0.26±0.10	0.02±0.02
	1-3	0.12±0.07	0.13±0.08	0.04±0.03
	3-9	0.04±0.04		0.04±0.03

B. Other possible sources for the $\Delta > 10$ -GeV events

1. $e^\pm\mu^\mp$ pairs from $e^+e^- \rightarrow e^+e^-\mu^+\mu^-$

The reaction in Eq. (7b) can produce $e^\pm\mu^\mp$ pairs in the tracking region of the detector. However, the Monte Carlo calculations described in Sec. IV A found zero events of this type compared to the 3000 e^+e^- and $\mu^+\mu^-$ pair events produced in the same calculations. Therefore this source was ignored.

2. Calculation for zero-photon events from $e^+e^- \rightarrow \tau^+\tau^-$

We used a Mark II Collaboration program called HOWLTAU to calculate by the Monte Carlo method the cross section and kinematic variable distributions for the zero-photon events from

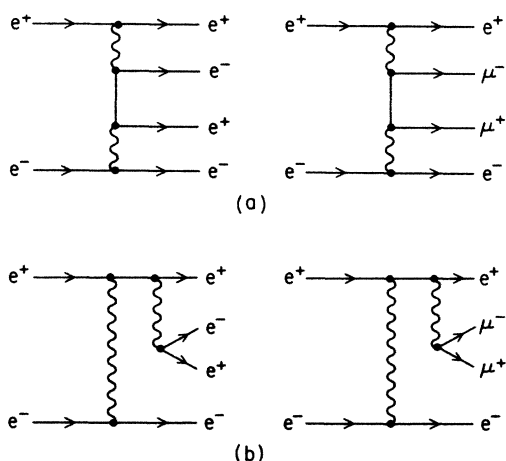


FIG. 11. Examples of Feynman diagrams for (a) the multiperipheral process, and (b) the bremsstrahlung process.

$$e^+e^- \rightarrow \tau^+ + \tau^-,$$

$$\tau^- \rightarrow \nu_\tau e^- \bar{\nu}_e, \nu_\tau \mu^- \bar{\nu}_\mu, \nu_\tau \pi^-, \nu_\tau K^-, \text{ or } \nu_\tau \pi^- K_L^0, \quad (8)$$

$$\tau^+ \rightarrow \bar{\nu}_\tau e^+ \nu_e, \bar{\nu}_\tau \mu^+ \nu_\mu, \bar{\nu}_\tau \pi^+, \bar{\nu}_\tau K^+, \text{ or } \bar{\nu}_\tau \pi^+ \bar{K}_L^0.$$

After the event-selection criteria of Sec. II C and the $\Delta > 10$ GeV requirement of this section are applied, the cross section is 1.7 ± 0.2 pb. This is small compared to the relevant $e^+e^- \rightarrow e^+e^-e^+e^-$, $e^+e^- \mu^+\mu^-$ cross sections in Table II. However, before we can ignore the cross section from the process in Eq. (8), we have to compare cross sections for the various values of m and p_T . This is done in Table III.

Considering the statistical errors in the Monte Carlo calculations we can ignore the $e^+e^- \rightarrow \tau^+\tau^-$ contribution except in the kinematic region $5 < m < 10$ GeV/ c^2 , $p_T > 3$ GeV/ c . Inside that region we shall add the $e^+e^- \rightarrow \tau^+\tau^-$ contribution to the still dominant $e^+e^- \rightarrow e^+e^-e^+e^-$, $e^+e^- \mu^+\mu^-$ cross sections.

3. $\pi^+\pi^-$ and K^+K^- pairs from $e^+e^- \rightarrow e^+e^-\pi^+\pi^-$, $e^+e^-K^+K^-$

The reaction

$$e^+ + e^- \rightarrow e^+ + e^- + \pi^+ + \pi^- \quad (9)$$

can contribute $\pi^+\pi^-$ pairs to be the observed data sample. Indeed we⁴ and other experimenters⁵ have studied events from this reaction to examine the process

$$\gamma_\nu + \gamma_\nu \rightarrow \pi^+ + \pi^-,$$

where γ_ν is a virtual photon. The same methods⁴ could be used in this data sample to measure $\pi^+\pi^-$ pair production, but our event-selection criteria are not felicitous for such a measurement. We require $\theta_{\text{coll}} > 20^\circ$ and emphasize large values of p_T and m . The studies of $\pi^+\pi^-$ production emphasize small values of p_T ; for example, Ref. 4 required $p_T < 0.3$ GeV/ c . Therefore in this work we do not attempt to separate out the $\pi^+\pi^-$ pairs. Analogous con-

siderations apply to K^+K^- pairs from the reaction

$$e^+ + e^- \rightarrow e^+ + e^- + K^+ + K^- . \quad (10)$$

4. Pairs from $e^+e^- \rightarrow \gamma\gamma e^+e^-$

The reaction

$$e^+ + e^- \rightarrow \gamma + \gamma + e^+ + e^- , \quad (11)$$

where neither photon is detected can contribute e^+e^- pairs to the data. We face both calculational and experimental difficulties in accurately determining this contribution. At present we do not have a computer program that can accurately calculate the cross section for the reaction in Eq. (11) for the event criteria used in this paper. We have used an approximate calculation⁶ (Appendix B) in which the photons are emitted only by the initial e^+ and e^- , and in which the transverse momentum of these photons is ignored. The experimental difficulty is caused by the incomplete photon detection of our detector; it would be difficult to determine the photon detection efficiency when θ_γ is larger than m_e/E_b but still small.

The right-most column of Table II gives the calculated cross section for $e^+e^- \rightarrow \gamma\gamma e^+e^-$ as calculated by the method in Appendix B. The restriction on θ_γ precludes p_T being outside the 0–1-GeV/c range. We observe that this cross section is small compared to the cross section for four-lepton production when $m < 10 \text{ GeV}/c^2$ and $p_T < 1.0 \text{ GeV}/c$. An approximate calculation using a computer program for $e^+e^- \rightarrow e^+e^- \gamma$ with initial-state radiation shows that this observation is true for all p_T as long as $m < 10 \text{ GeV}/c^2$.

When $m > 10 \text{ GeV}/c^2$ the $e^+e^- \rightarrow \gamma\gamma e^+e^-$ cross section is the same size as the four-lepton cross sections. We will return to this point in the next section when we discuss the data with $m > 10 \text{ GeV}/c^2$.

C. Comparison of data with calculations

We are now ready to compare the $\Delta > 10 \text{ GeV}$ data with the calculated cross sections for $e^+e^- \rightarrow e^+e^-e^+e^-$, $e^+e^- \mu^+\mu^-$. Table IV lists the types of observed particle pairs. The category of ambiguous particles is divided into μ/h meaning μ or h , e/h meaning e or h , and $e/\mu/h$ meaning e or μ or h . (There is no e/μ category in our particle-identification method because if we cannot identify a particle as an e or a μ we

TABLE IV. Classification of pairs according to the type of particle. e , μ , and h mean electron, muon, and hadron, respectively. μ/h means μ or h , e/h means e or h , and $e/\mu/h$ means e or μ or h .

	e	μ	h	μ/h	e/h	$e/\mu/h$
e	551	5	29	33	128	252
μ		232	35	364	6	49
h			8	33	7	15
μ/h				436	6	172
e/h					16	30
$e/\mu/h$						62

cannot show it is not an h , hence e/μ is included in $e/\mu/h$.) The data in Table IV and our HOWL Monte Carlo program simulation of the Mark II detector give the average probability of identifying an e as an e to be

$$P_e = 0.74 \pm 0.05 ,$$

where the error is due to systematic uncertainties. We do not attempt to evaluate a similar quantity for muons because the muon-identification system is quite limited in its angular acceptance and has a unfavorable momentum dependence for this data. Hence we do not attempt to separate out hh pairs. Considering the misidentification probabilities in our detector for low-momentum particles, Table IV is consistent with all events being ee or $\mu\mu$ pairs, and there are less than 15% hh pairs. Therefore we proceed, considering the data to be mainly composed of ee and $\mu\mu$ pairs. Since the predicted $e^+e^-e^+e^-$ and $e^+e^- \mu^+\mu^- p_T$ and m distributions are so similar (Table III) we add them together and then compare them with all the data (Figs. 12 and 13). We postpone the separation of the ee pairs and $\mu\mu$ pairs until the end of this section. The calculation of the measured cross section involves the corrections for detector resolution and inefficiency, and the systematic errors discussed in Appendix C.

In the plot of $d\sigma/dm$ vs m (Fig. 12), the measured and calculated cross sections agree within the statistical and systematic errors. When $m > 2 \text{ GeV}/c^2$, $d\sigma/dm$ decreases rapidly as m increases, by a factor of 100 as m reaches $10 \text{ GeV}/c^2$. The decrease in $d\sigma/dm$ when $m < 2 \text{ GeV}/c^2$ is caused by our criterion that each track have $p > 1.0 \text{ GeV}/c$.

Figure 13 shows $d\sigma/dp_T$ vs p_T for the main mass

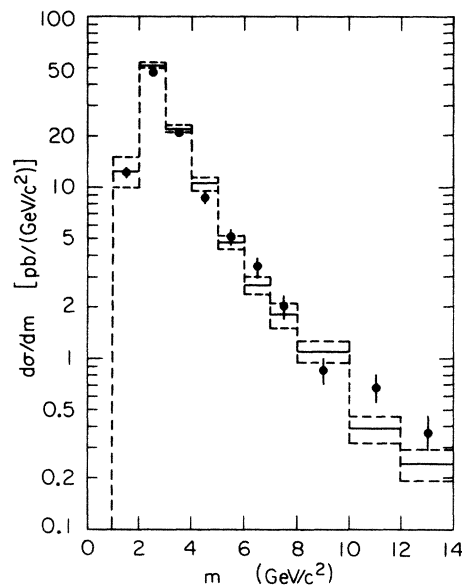


FIG. 12. The cross section $d\sigma/dm$ as a function of m . The data is given by the points, the error bars show ± 1 standard deviation of statistical error. An overall systematic error of $\pm 8\%$ is not shown. The histogram gives the average value (solid line) and ± 1 standard deviation (dashed lines), for the Monte Carlo calculation of $d\sigma/dm$ for the sum of the processes $e^+e^- \rightarrow e^+e^-e^+e^-$, $e^+e^- \mu^+\mu^-$, $\tau^+\tau^-$, $\gamma\gamma e^+e^-$.

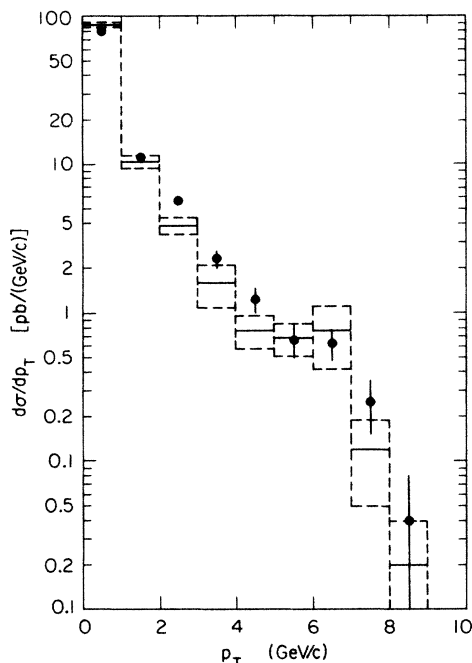


FIG. 13. The cross section $d\sigma/dp_T$ as a function of p_T for $1 < m < 10 \text{ GeV}/c^2$. The data are given by the points, the error bars show ± 1 standard deviation of statistical error. An overall systematic error of $\pm 8\%$ is not shown. The histogram gives the average value (solid line) and ± 1 standard deviation (dashed lines) for the Monte Carlo calculation of $d\sigma/dp_T$ for the sum of the process $e^+e^- \rightarrow e^+e^-e^+e^-$, $e^+e^-\mu^+\mu^-$, $\tau^+\tau^-$, $\gamma\gamma e^+e^-$.

range of $1 \leq m \leq 10 \text{ GeV}/c^2$. There is a rapid falloff of $d\sigma/dp_T$ with increasing p_T . This behavior and that illustrated in Fig. 12 are characteristic of the kinematics of the reactions $e^+e^- \rightarrow e^+e^-e^+e^-$, $e^+e^-\mu^+\mu^-$ when just two particles are observed at large angles to the beam line.

To examine the joint p_T - m distribution and continue

TABLE V. The experimental cross section σ_{expt} for all data; the calculated cross section σ_{calc} for the sum of the processes $e^+e^- \rightarrow e^+e^-e^+e^-$, $e^+e^-\mu^+\mu^-$, $\tau^+\tau^-$, $\gamma\gamma e^+e^-$; the ratio $\rho = \sigma_{\text{expt}}/\sigma_{\text{calc}}$; and the difference $\delta = \sigma_{\text{expt}} - \sigma_{\text{calc}}$. One standard deviation statistical errors for the data and the Monte Carlo calculations are given. The second error on σ_{expt} , ρ , and δ is the systematic error. An additional decimal place in the σ 's, not shown here, was used to calculate ρ and δ .

m range (GeV/c^2)	p_T range (GeV/c)	σ_{expt} (pb)	σ_{calc} (pb)	ρ	δ (pb)
1-2	0-1	$8.7 \pm 0.6 \pm 0.7$	10.1 ± 1.9	$0.86 \pm 0.18 \pm 0.07$	$-1.5 \pm 2.0 \pm 0.7$
	1-3	$3.0 \pm 0.4 \pm 0.3$	1.3 ± 0.6	$2.3 \pm 1.1 \pm 0.2$	$1.7 \pm 0.7 \pm 0.3$
	3-9	$0.5 \pm 0.2 \pm 0.04$	1.0 ± 0.6	0.5^a	$-0.5 \pm 0.6 \pm 0.04$
2-3	0-1	$42.0 \pm 1.3 \pm 3.5$	47.5 ± 1.6	$0.88 \pm 0.04 \pm 0.07$	$-5.5 \pm 2.1 \pm 3.5$
	1-3	$4.3 \pm 0.4 \pm 0.4$	4.2 ± 0.5	$1.03 \pm 0.16 \pm 0.09$	$+0.1 \pm 0.7 \pm 0.4$
	3-9	$1.1 \pm 0.2 \pm 0.1$	0.5 ± 0.2	$2.3 \pm 1.1 \pm 0.2$	$+0.6 \pm 0.3 \pm 0.1$
3-5	0-1	$22.2 \pm 1.0 \pm 1.9$	25.3 ± 1.0	$0.88 \pm 0.05 \pm 0.07$	$-3.1 \pm 1.4 \pm 1.9$
	1-3	$6.5 \pm 0.5 \pm 0.5$	6.2 ± 0.5	$1.04 \pm 0.12 \pm 0.09$	$+0.2 \pm 0.7 \pm 0.5$
	3-9	$0.9 \pm 0.3 \pm 0.07$	1.2 ± 0.2	$0.71 \pm 0.20 \pm 0.06$	$-0.4 \pm 0.3 \pm 0.07$
5-10	0-1	$6.5 \pm 0.5 \pm 0.5$	7.1 ± 0.5	$0.92 \pm 0.10 \pm 0.08$	$-0.6 \pm 0.7 \pm 0.5$
	1-3	$3.1 \pm 0.4 \pm 0.3$	2.8 ± 0.3	$1.11 \pm 0.18 \pm 0.09$	$+0.3 \pm 0.5 \pm 0.3$
	3-9	$2.6 \pm 0.3 \pm 0.2$	1.6 ± 0.3	$1.64 \pm 0.33 \pm 0.14$	$+1.0 \pm 0.4 \pm 0.2$
10-15	0-1	$0.8 \pm 0.2 \pm 0.07$	1.0 ± 0.1	$0.8 \pm 0.2 \pm 0.07$	$-0.2 \pm 0.2 \pm 0.07$
	1-3	$0.8 \pm 0.2 \pm 0.06$	0.3 ± 0.1	2.6^a	$+0.5 \pm 0.2 \pm 0.06$
	3-9	$0.7 \pm 0.2 \pm 0.06$	0.08 ± 0.05	8.9^a	$+0.6 \pm 0.2 \pm 0.06$

^aThe large fractional error in σ_{calc} precludes a meaningful standard deviation in ρ .

the comparison, we define, for the experimental cross sections σ_{expt} and the calculated cross section σ_{calc} , the ratio of experiment to theory:

$$\rho(p_{T1} < p_T < p_{T2}, m_1 < m < m_2) = \frac{\sigma_{\text{expt}}(p_{T1} < p_T < p_{T2}, m_1 < m < m_2)}{\sigma_{\text{calc}}(p_{T1} < p_T < p_{T2}, m_1 < m < m_2)}. \quad (12)$$

Table V gives ρ , the statistical error combines the statistical errors of σ_{expt} and σ_{calc} , the systematic error is from σ_{expt} . In almost all kinematic regions ρ is 1.0 within the sometimes large errors. There is perhaps a deviation from 1.0 in the $m > 10 \text{ GeV}/c^2$, $p_T > 1 \text{ GeV}/c$. We cannot determine if this is caused by the contamination of class-2 events by class-1 events (Sec. III C); by our limited calculation of the cross section for $e^+e^- \rightarrow \gamma\gamma e^+e^-$ (Appendix B); or if there is some other reason for the apparent deviation. Thus, excepting the aforementioned kinematic region, the bulk of the events are explained by the reactions discussed in Secs. IV A and IV B.

One check of this conclusion remains to be done. Looking at Table III, we expect the experimental e^+e^- pair cross section $\sigma_{\text{expt},ee}$ to be about equal to the experimental $\mu^+\mu^-$ pair cross section, when $m < 10 \text{ GeV}/c^2$. It is convenient to define the ratio

$$r_{ee} = \sigma_{\text{expt},ee} / \sigma_{\text{expt}} \quad (13)$$

and we expect that $r_{ee} \approx 0.42-0.5$ depending on the fraction of hadron pairs. The calculation of $\sigma_{\text{expt},ee}$ involves the efficiencies and systematic errors listed in Appendix C. Table VI gives the measured values of r_{ee} , which tend to be smaller than 0.5, more in the range of 0.4-0.5. The systematic error on the identification of ee pairs and the correction for detector losses relative to those quantities for any pair is large (Appendix C). Therefore, we cannot conclude that these smaller values of r_{ee} are significantly different from 0.5.

TABLE VI. The ratio $r_{ee} = \sigma_{\text{expt}, ee} / \sigma_{\text{expt}}$. The first error is statistical, the second is systematic.

m range (GeV/ c^2)	p_T range (GeV/ c)	r_{ee}
1–2	0–1	$0.38 \pm 0.05 \pm 0.04$
	1–3	$0.44 \pm 0.10 \pm 0.05$
	3–9	$0.47 \pm 0.25 \pm 0.05$
2–3	0–1	$0.43 \pm 0.03 \pm 0.05$
	1–3	$0.49 \pm 0.09 \pm 0.05$
	3–9	$0.38 \pm 0.15 \pm 0.05$
3–5	0–1	$0.48 \pm 0.04 \pm 0.05$
	1–3	$0.43 \pm 0.06 \pm 0.05$
	3–9	$0.32 \pm 0.15 \pm 0.04$
5–10	0–1	$0.50 \pm 0.07 \pm 0.05$
	1–3	$0.51 \pm 0.11 \pm 0.06$
	3–9	$0.64 \pm 0.13 \pm 0.07$

Taking a final overall look at the ratios ρ and r_{ee} in Tables V and VI, the comparison of data and theory does not turn out as nice as one might wish. In the $0 < p_T < 1$ GeV/ c region where the statistical errors are smallest, there seems to be a deficit of events, if we accept the calculated cross sections as correct. But our systematic errors preclude further investigation.

D. Limits on unconventional processes

Having found the explanation for the bulk of the events, we finally consider the limits on unconventional processes that would yield charge-particle pairs and no other particles in the fiducial volume of our detector. We measure the limit by defining

$$\delta = \sigma_{\text{expt}} - \sigma_{\text{calc}}; \quad (14)$$

δ is given in Table V. Its values both positive and negative range from several pb to a fraction of a pb. They are all consistent with zero within the statistical and systematic errors. The utility of upper limits on cross sections at the pb level depends upon the unconventional reaction being considered. At our energy, 29 GeV, the electromagnetic annihilation cross section for one unit of R is about 100 pb. On the other hand, the weak annihilation cross section into an $L^0 \bar{L}^0$ pair³ is about one-third of a pb. Hence the limits given in Table V are not nearly as small as we would like; this leads to conclusion (4) in the next section.

V. CONCLUSIONS

We have carried out the first systematic study of noncollinear, two-charged-particle events produced at high energy in electron-positron annihilation. We required that the particles be noncollinear by at least 20° , that there be no detected isolated photons, and that the kinematics indicate two or more undetected particles. Our motivation was first to see if the events could be explained by known reactions; and second to see if there was evidence for, or to determine what limits could be put on, unconventional reactions.

We draw four conclusions from the figures, tables, and

discussion in Secs. III and IV.

(1) The kinematic-variable distributions and cross sections of the $\Delta > 10$ GeV, $1 \leq m \leq 10$ GeV/ c^2 events can be explained by the bulk of the events coming from the reactions $e^+e^- \rightarrow e^+e^-e^+e^-$ and $e^+e^- \rightarrow e^+e^-\mu^+\mu^-$.

(2) The reactions $e^+e^- \rightarrow e^+e^-\pi^+\pi^-$, $e^+e^- \rightarrow e^+e^-K^+K^-$, $e^+e^- \rightarrow \tau^+\tau^-$ (two-prong, zero-photon), and $e^+e^- \rightarrow \gamma\gamma e^+e^-$ may also contribute events, but their cross sections are small compared to the four-lepton cross sections in the kinematic regions studied in this paper. In general the existence of these smaller contributions cannot be confirmed.

(3) The bulk of the events are explained by conclusion (1), but statistical errors and systematic errors make it impossible to exclude unconventional sources for a fraction of the cross section. The limits on a cross section from an unconventional source are at the pb level (Table V).

(4) Further investigation of the physics considered here requires (a) a detector with more complete photon detection and with particle tracking over a larger solid angle, and (b) a complete calculation of the reaction $e^+e^- \rightarrow \gamma\gamma e^+e^-$.

ACKNOWLEDGMENTS

We are greatly indebted to the work of F. A. Berends, P. H. Daverveldt, and R. Kleiss. This work was supported in part by the Department of Energy under Contracts Nos. DE-AC03-76SF00515 (SLAC), DEAC03-76SF00098 (LBL), and DE-AC02-76ER03064 (Harvard).

APPENDIX A: SHAPE OF THE MEASURED Δ DISTRIBUTION IN $e^+e^- \rightarrow e^+e^-\gamma$

The width of the Δ distribution for $e^+e^- \rightarrow e^+e^-\gamma$ in Fig. 9 comes primarily from the errors in the measurement of the momenta p_1 and p_2 . The standard deviation is

$$\sigma_p = \{p[(0.2)^2 + (0.01p)^2]^{1/2} / \sin\theta\} \text{ GeV}/c, \quad (A1)$$

where θ is the polar angle of \mathbf{p} and p is in GeV/ c .

For example, if \mathbf{p}_1 and \mathbf{p}_2 are approximately collinear and larger than several GeV/ c , the error in p_{miss} from Eq. (4a) is

$$\sigma_{p_{\text{miss}}} \approx [0.01(p_1^2 + p_2^2)^{1/2} / \sin\theta] \text{ GeV}/c.$$

The error in Δ is

$$\sigma_\Delta \approx [0.02(p_1^2 + p_2^2)^{1/2} / \sin\theta] \text{ GeV}. \quad (A2)$$

Thus two 10-GeV/ c particles have $\sigma_\Delta \approx (2.8/\sin\theta)$ GeV. Since most of the $e^+e^-\gamma$ events in Fig. 9 have p_1 and p_2 in the range of 5–15 GeV/ c , the half-width of the distribution is several GeV.

The tail of the distribution for $\Delta > 10$ GeV is the sum of the effect of the large σ_Δ and the inclusion of $e^+e^- \rightarrow e^+e^-\gamma\gamma$ where one γ is not detected.

APPENDIX B: CALCULATION OF THE CROSS SECTION FOR $e^+e^- \rightarrow \gamma\gamma e^+e^-$

We used Ref. 6 to calculate the cross section for

$$e^+e^- \rightarrow \gamma + \gamma + e^+ + e^- \quad (B1)$$

in the approximation that the photons are emitted only by the incident e^+ and e^- , and that the transverse momenta of the photon can be neglected. The differential cross section is

$$\frac{d^3\sigma}{dw_1 dw_2 d\Omega^*} = F(w_1)F(w_2) \frac{\alpha^2(\hbar c)^2}{4m^2} \times \left(\frac{3 + \cos\theta^*}{1 - \cos\theta^*} \right)^2. \quad (\text{B2})$$

Here w_1 and w_2 are the energies of the emitted photons in the laboratory frame, m is the invariant mass of the final e^+e^- pair, θ^* is the polar angle of the final e^- relative to the e^- in the final e^+e^- barycentric frame, and $d\Omega^*$ is the differential solid angle in that frame. The constants are the fine-structure constant α , the Planck constant \hbar , and the velocity of light c :

$$F(w) = \frac{2\alpha}{\pi} \frac{1}{w} \left[1 - \frac{w}{E_b} + \frac{w^2}{2E_b} \right] \ln \left[\frac{E_b}{m_e} \right]. \quad (\text{B3})$$

Here E_b is the beam energy and m_e is the electron mass.

A Monte Carlo computer program is used to calculate the cross section for the various m intervals. Since the transverse momenta of the photons is ignored, p_T is always zero.

APPENDIX C: CORRECTIONS FOR DETECTOR INEFFICIENCY AND RESOLUTION, AND SYSTEMATIC ERRORS

1. Relative efficiency

The Mark II Monte Carlo detector simulator program HOWL was used to correct for detector inefficiency and resolution.

Define N_{theory} as the number of events predicted by the Berends, Daverveldt, and Kleiss¹ programs for the *event criteria* of Sec. II C with $\Delta > 10$ GeV in a perfect detector. Define N_{observe} as the number we would expect to observe

in the Mark II detector. Then define the relative efficiency

$$E = N_{\text{observe}} / N_{\text{theory}}.$$

We find the average values of E to be

$$\mu^+\mu^- \text{ pairs, } E_{\mu\mu} = 0.95;$$

$$e^+e^- \text{ pairs, } E_{ee} = 0.85;$$

$$h^+h^- \text{ pairs, } E_{hh} = 0.91.$$

The principal reason for $E_{ee} < E_{\mu\mu}$ is that the electrons lose more energy than the muons as they pass through the detector material. There is about a 5% chance that an electron produced with $p > 1.0$ GeV/ c will lose sufficient energy so as to yield a measured p below the 1.0-GeV/ c criterion. Thus there is about a 10% greater chance that an e^+e^- pair will not be counted within the event criteria.

An analysis of the event-type data in Table IV shows that the *produced* events have about equal numbers of e^+e^- and $\mu^+\mu^-$ pairs and less than 15% other pairs: h^+h^- , $e^\pm\mu^\mp$, $e^\pm h^\mp$, $\mu^\pm h^\mp$. The overall value of E is

$$E_{\text{all}} = 0.90.$$

2. Systematic errors

The percent systematic error in E_{all} due to uncertainties in the detector simulation is $\pm 6\%$. The other major systematic uncertainty is in the total luminosity, and is $\pm 5\%$. For convenience we use these in quadrature, namely, $\pm 8\%$; but, of course, they could add linearly. This $\pm 8\%$ is used for the systematic error in σ_{expt} , ρ , and δ in Table V; and it is noted in the captions of Figs. 12 and 13.

The systematic error in r_{ee} (Sec. IV C) does not involve the luminosity uncertainty; but it does involve an uncertainty in E_{ee} which is not correlated with an uncertainty in $E_{\mu\mu}$; and it also involves the uncertainty in P_e . The total systematic error on r_{ee} is $\pm 11\%$.

^(a)Present address: University of Pennsylvania, Philadelphia, PA 19104.

^(b)Present address: CERN, CH-1211, Geneva 23, Switzerland.

^(c)Present address: Oxford University, Oxford, England.

^(d)Present address: University of Chicago, Chicago, IL 60637.

^(e)Present address: Therma-Wave Corp., Fremont, CA 94539.

^(f)Present address: California Institute of Technology, Pasadena, CA 91125.

^(g)Present address: Fermilab, Batavia, IL 60510.

^(h)Present address: Laboratoire de Physique Nucléaire et Hautes Energies, Université Pierre et Marie Curie, F-75230 Paris, France.

⁽ⁱ⁾Present address: Stanford Linear Accelerator Center, Stanford, CA 94305.

¹F. A. Berends, P. H. Daverveldt, and R. Kleiss, Nucl. Phys. **B253**, 441 (1985).

²P. H. Daverveldt, Proefchrift, Rigksuniversiteit te Leiden (1985).

³M. L. Perl *et al.*, Phys. Rev. D **32**, 2859 (1985).

⁴J. Boyer *et al.*, Phys. Rev. Lett. **56**, 207 (1985); J. R. Smith *et al.*, Phys. Rev. D **30**, 851 (1984).

⁵For a review, see H. P. Paar, in *Physics in Collision 4*, proceedings of the Fourth International Conference, Santa Cruz, 1984, edited by A. Seiden (Editions Frontieres, Gif-sur-Yvette, France, 1985), p. 339.

⁶V. N. Baier, V. S. Fadin, and V. A. Khoze, Nucl. Phys. **B65**, 381 (1973).